Submitted to Materials Science and Engineering A (October 2021)

Fabrication of hybrid nanocrystalline Al-Ti alloys by mechanical bonding through high-pressure torsion

Piotr Bazarnik[a,1], Aleksandra Bartkowska[b,1*] Yi Huang[c,d], Karol Szlązak[a], Bogusława Adamczyk-Cieślak[a], Jordi Sort[b,e], Malgorzata Lewandowska[a], Terence G. Langdon[d]

[a] Warsaw University of Technology, Faculty of Materials Science and Engineering, Woloska 141, 02-507, PL
[b] Departament de Física, Universitat Autònoma de Barcelona, 08193 Bellaterra, Spain
[c] Department of Design and Engineering, Faculty of Science and Technology, Bournemouth University, Poole, Dorset BH12 5BB, UK
[d] Materials Research Group, Department of Mechanical Engineering, University of Southampton, Southampton SO17 1BJ, UK
[e] Institució Catalana de Recerca i Estudis Avançats (ICREA), Passeig Ll. Companys 23, 08010 Barcelona, Spain

Abstract

This study demonstrates an approach of utilizing high-pressure torsion (HPT) to fabricate a novel hybrid material by the direct bonding of Al and Ti disks at room temperature under a compressive pressure of 6.0 GPa and with increasing numbers of HPT turns up to 50. Detailed structural observations revealed the formation of a multi-layered nanostructure in the edge regions of the disks with a grain size of ~30 nm. X-ray diffraction (XRD) and selected area electron diffraction (SAED) confirmed the presence of three intermetallic compounds, AlTi, Al_3Ti and Ti_3Al, in the layered structures. Processing by HPT led to the formation of a hybrid nanocomposite with exceptional hardness (over 300 Hv) in the edge regions of the disks. Special emphasis was placed on understanding the evolution of hardness in the hybrid material. The investigation demonstrates a significant opportunity for using HPT processing to deepen the knowledge on diffusion bonding and mechanical joining technologies as well as for fabricating new and valuable hybrid nanomaterials.

Keywords: high-pressure torsion, hybrid materials, titanium, aluminium, ultrafine grains.

*Corresponding author: Aleksandra Bartkowska (e-mail: aleksandra.bartkowska@uab.cat)

1 P.Bazarnik and A.Bartkowska contributed equally to this work as first authors

1. Introduction

High-pressure torsion (HPT) is a severe plastic deformation (SPD) technique which enables scientists to achieve truly nanometric-sized grains by a simultaneous combination of large compressive stresses (typically several GPa) and torsional forces [1–3]. In the HPT method, a sample in the form of a thin disk is placed between two solid anvils and compressed under a pressure of several GPa at room or an elevated temperature. At the same time, the sample is subjected to torsional strain initiated by the rotation of one of the anvils with respect to the other. Frictional forces prevent any sliding between the disk sample and the anvils, therefore allowing torsional deformation applied onto the disk sample.

The equivalent strain (von Mises strain) ε_{eq} imposed on the sample in the form of a disk in HPT is described by an Eq.1 below [4]:

$$\varepsilon_{eq} = \frac{2\pi N r}{h\sqrt{3}} \quad (1)$$

where *N* is the number of HPT revolutions (turns), *r* is the radial distance from the centre of the disk and *h* is the final thickness of the sample. Analysis of Eq.1 shows there is a variation in the strain value across the disk, with the maximum value on the edge and the minimum in the centre of the disk (in theory $\varepsilon_{eq}=0$ as r=0). Therefore, according to the equation HPT-processed materials will show inhomogeneous microstructures and properties. On the other hand, it is possible to fabricate materials with reasonably homogeneous microstructures as reported elsewhere [3].

The advantage of the HPT method is undoubtedly the possibility of applying very large strains through a sufficiently high number of HPT turns, where this strain is much larger than in other severe plastic deformation methods. However, there is a certain limitation regarding the minimum grain size that may be attained via SPD processing as well as any associated improvement in the mechanical properties [5,6]. Depending on the type of metal subjected to HPT processing, three main types of behaviour may be identified: strain hardening, strain softening with recovery and strain softening without recovery [5–7]. The dominant types of metals demonstrate the strain hardening type of behaviour, associated with a significant increase in mechanical properties during deformation up to some saturation level [5,6]. However, the enhanced mechanical properties are usually combined with a reduction in plasticity which significantly limits the possible application of HPT-processed materials [5,6]. On the other hand, in materials exhibiting strain softening, such as pure aluminium, it is not possible to obtain true ultrafine-grained and nanograined structure because of the recovery processes taking place during plastic deformation [6,8–10]. Nonetheless, they are showing relatively good plasticity associated with a modest increase in mechanical properties resulting from a fractional decrease in grain size which in turn tends to eliminate those materials from industrial applications.

The potential solution to overcome the limits of grain refinement and enhancement in mechanical properties lies in developing a new class of hybrid materials fabricated by HPT [11–18]. In this approach two or more dissimilar metals are joined through HPT to obtain a multilayered hybrid material with new and unique properties. Since this is a new approach, there is to date only a limited number of scientific reports focused on the fabrication of high-performance materials by bonding dissimilar bulk metals to form a new metal system through HPT. The first report demonstrated the potential for forming a spiral texture by processing of an Al-Cu hybrid material though HPT using four quarter-disks, including two of pure Cu and two of an Al-6061 alloy [19]. However, this study described only the computational calculation

of the distribution of equivalent stress in the processed disk using a finite element method and there was no detailed microstructural analysis and mechanical testing of the processed disk. Later, this approach was improved and further developed by bonding of separate Al and Mg disks processed through HPT by stacking a set of two or three disks [20,21] producing multi-layered nanostructures. This same approach was used in several other investigations using stacks of three or more disks of Al-Cu [18,22–24], Cu-Ta [25], Zn-Mg [26,27], Fe-V [28], Cu-Sn [29], Zr-Nb [30].This series of research investigations proved that HPT is a good technique to create a strong bonding of the dissimilar metal disks. Moreover, for higher numbers of HPT revolutions a strong tendency for segregation was observed with the nucleation of intermetallic compounds through diffusion bonding. This led to a significant increase of hardness which was higher than may be achieved for the initial metals.

Accordingly, the present work was initiated to evaluate the microstructural changes and the mechanical properties evolution in the Al-Ti system synthesized by the HPT procedure to high number of turns (up to 50 revolutions). In particular, the investigation is designed to examine the extent of microstructural refinement, the formation and decomposition of composite microstructures during deformation, the formation of any intermetallic compounds and their impact on the subsequent mechanical properties.

2. Experimental materials and procedures

A bulk nanocrystalline Al-Ti hybrid material was prepared by mechanical bonding of a commercial purity aluminium Al (Al-1050 alloy) and a commercial purity titanium (CP-Ti). Both alloys were received as extruded rods with diameters of 10 mm. Those rods were cut into a series of disks with thicknesses of around 1 mm and then the disks were polished to final thicknesses of 0.3 and 0.15 mm for Al and Ti, respectively. Hybrid materials were synthesised using conventional HPT processing with the exception that the straining was applied to a stack of a few disks instead of one as described in an earlier study [31]. A stack of three Al and two Ti disks were processed through HPT at room temperature under quasi-constrained conditions [32] with a constant speed of 1 rpm and under an applied pressure of 6.0 GPa, for total numbers of revolutions N of 10, 20, 30, 40 and 50. Each anvil had a cavity depth 0.25 mm and the final thickness of sample was about 0.8 mm. In addition, Al-1050 and Ti samples in the initial state and after HPT processing for 10 revolutions were used as reference samples.

The HPT-processed disks were initially examined by X-ray diffraction (XRD) using Bruker D8 Discover and an energy for the emitter beam of 30 kV. The filtered Co Kα X-Ray radiation was focussed to a point with a radius of 1 mm and all specimens were scanned on cross-sectional planes in the edge regions. Each sample was illuminated by high intensity hard X-rays for 5 s per step, the 2Θ angle was between 20° and 90° and the step size Δ2Θ was 0.025°.

After processing by HPT, each disk was cut vertically along a randomly selected diameter to obtain two semi-circular disks. One vertical cross-section from each disk was mounted in resin, ground and polished to obtain a mirror-like surface. Then, samples were examined using light microscopy (LM) with a Zeiss Axio Observer. Panoramic photos of the overall cross-sections were made in order to provide preliminary information on the quality of bonding between the individual components. To prepare the panoramic images, a series of photos were made and then placed together to give an overall perspective.

In order to evaluate the quality of bonding between the Al and Ti elements a scanning electron microscope (SEM) Hitachi SU8000 was used. In addition, maps of the chemical compositions were recorded for selected samples using the energy-dispersive X-ray spectroscopy (EDX) technique. SEM investigations were conducted in two modes: secondary

electron mode (SE) and backscattered electron mode (BSE) on the cross-sections of disks. Microstructural observations were carried out in the peripheral regions (approximately 1.0 mm from the edge) of each disk. Specimens for SEM analysis were prepared using Hitachi IM4000 ion milling system. In practice, ion milling is a damage-less process and the polishing with an ion beam eliminates all deformation, stresses and oxide layers. Moreover, the surface quality is sufficiently good that it is possible to observe the structure of such prepared joints through the channelling contrast in an SEM.

Detailed microstructural analysis was carried out using a transmission electron microscope (TEM) JEOL JEM 1200 operating at an accelerating voltage of 120 kV and CS-corrected dedicated scanning transmission electron microscope (STEM) Hitachi HD2700, operating at 200 kV. Samples for TEM/STEM observations were prepared using a Focused Ion Beam (FIB) Hitachi NB-5000 microscope. The lamellas were cut from the cross-section of the sample in the direction parallel to the direction of rotation. STEM observations were carried out in bright-field (BF) and high-angle annular dark field (HAADF) modes. For selected samples, selected area electron diffraction (SAED) patterns were obtained.

The microstructures were evaluated quantitatively using a computer-aided image analyser. The grain sizes were described in terms of the equivalent grain diameter, d_{eq}, defined as the diameter of a circle with a surface area equal to the surface area of the grain.

Micro-computed tomography (microCT) was performed on the samples by means of a SkyScan 1172 (Bruker, USA), in order to investigate the microstructural distribution of the material constituents. For this purpose, the source voltage and source current were set to 100 kV and 100 μA, respectively. Al+Cu X-Ray filters were used. The obtained pixel sizes were 5 and 2 μm, the scanning procedures were carried out by performing a rotation of the emitted X-ray by 180°, with a step size of 0.3° and 0.2°, and an exposure time of 580 ms and 600 ms per projection for the 10 turns and 50 turns samples, respectively.

To examine the mechanical properties of the samples, microhardness and nanoindentation tests were performed. The microhardness measurements were carried out using a Zwick/Roell Z2.5 hardness testing machine with a load of 200 g. The hardness of the initial materials was measured as well as EDX linear analysis, conducted in the middle of cross-sections of the initial samples after HPT processing (Al-1050 and Ti after 10 revolutions). For the linear analysis, the distances between consecutive measurement points were 0.2 mm. Hardness maps of selected samples of the Al-Ti hybrid materials were prepared applying the distances between consecutive measurements points of 0.1 mm. Measurements were carried out on the cross-sections of selected samples and the microhardness data were then used to prepare colour-coded contour maps displaying the hardness distributions within each disk.

Microhardness measurements were complemented by nanoindentation studies conducted using an Anton Paar device operating in the load-control mode with a Berkovich pyramidal-shaped diamond tip. The value of the maximum applied force was chosen to be 50 mN to allow for measurements within the thin mixing layers of the hybrid material. To obtain reliable values of mechanical properties, at least 20 tests were measured per sample/condition. A series of measurements were performed in the peripheral areas for the hybrid material processed for 50 turns and HPT-processed CP-Ti as well as for Al-1050 in the as-received and HPT-processed state. The reduced Young's modulus (E_r) and hardness (H) were obtained from the load-displacement curves using the method of Oliver and Pharr [33]. The elastic and plastic energies of deformation were measured and the contribution of each in the total energy of deformation was then calculated. The elastic energy was obtained from the area enclosed between the unloading indentation segment and the displacement axis, whereas the plastic energy was assessed from the area between the loading and unloading indentation segments and the displacement axis.

3. Experimental results

3.1.Microstructures of HPT-processed hybrid materials

The LM images, prepared on cross-sections of 5-layered Al-Ti systems, are presented in Fig. 1 after deforming through various number of turns. In the samples after 10 and 20 turns, there are bent and fragmented Ti plates in the Al matrix without any significant mixing between the two components. There is also evidence for some delamination between the Ti and Al disks. Increasing the numbers of revolutions up to 50 gradually leads to a refinement of the two components and their mixing, and to a general elimination of any cracks and delaminations in the disks. However, even after 50 HPT turns the structure remains inhomogeneous, with visible differences between the edge and the centre of the disks. In the sample processed for 50 turns, the Ti and Al parts are indistinguishable in the edge area, which suggests the occurrence of a strong mixing between those elements. In addition, increasing the numbers of revolutions gradually leads to an expansion of the Al-Ti mixing zone in the sample, which is well observed when comparing images of samples processed from 30 to 50 turns as the area where large Ti fragments are present decreases in favour of an increase in the mixing zone of Al and Ti.

To gain a deeper understanding of the joining and mixing phenomenon which occurs in this system during HPT processing, the composites were further investigated using micro-computed X-ray tomography. This non-destructive characterization technique permits observations of new features that are generally invisible with more conventional imaging techniques such as LM or SEM analysis. The MicroCT 3D-reconstruction (in three planes: x-z, y-z and x-y-z) of the Al-Ti composites after 10 and 50 revolutions are presented on Figs 2 and 3 respectively. Fig. 2 a and b show the scan of a quarter of the HPT disk after 10 HPT turns which corresponds to about 13.4 mm^3 of material. It is apparent that torsional straining by HPT led to a bending, necking and finally to a fragmentation of the Ti phase (marked as red) across the disk diameter. This fragmentation effect is more intense with increasing numbers of turns which is evident after 50 HPT turns (Fig. 3 a, b and c). To show more details, a smaller volume of material from a mid-section of the disk was selected for the analysis (0.52 mm^3) but the analysis itself was conducted with a higher resolution. It should be noted that this MicroCT technique is not adequate for showing elements smaller than 1-2 μm. Nevertheless, the MicroCT reconstruction of the sample after 50 turns shows intense fragmentation of the Ti phase and its uniform distribution within the Al matrix.

Detailed microstructural observations were conducted using SEM, as shown by the SEM images in Fig. *4* andFig. 5 SEM images of the Al-Ti sample processed for 50 turns. where the brighter contrast represents the regions enriched in Ti and the darker contrast corresponds to the Al-rich regions. Fig. 4 shows detailed SEM images of the samples processed for 10 (a) and 20 (b,c) turns with visible delaminations and discontinuities between components as indicated by the red arrows but with no noticeable mixing between Al and Ti because the interfaces between the Al and Ti components are readily distinguishable. At the same time there is a strong bending of Ti layers inside the Al matrix and this becomes more intense with increasing

numbers of turns. It is apparent that 10 and 20 rotations are not sufficient to fully bond the components and therefore further processing was applied to higher numbers of turns.

Increasing the numbers of rotations up to 50 turns produces a severe fragmentation of the disks with a more homogeneous distribution of fragments of Ti in the Al matrix at the edge regions, as illustrated in Fig. 5 SEM images of the Al-Ti sample processed for 50 turns. It is readily apparent that after 50 turns the dominant part of the sample consists of relatively small fragmented parts of the Ti disk in the Al matrix, as shown in Fig. 5a. Increasing the numbers of revolutions up to 50 turns therefore permits a reduction in the sizes of the areas enriched in Ti. The red arrows in Fig. 5a,c indicate regions with enhanced mixing where the BSE contrast changes, suggesting a mixing between Al and Ti and the formation of intermetallic phases. As confirmed by both LM, MicroCT and SEM observations, the numbers of large Ti fragments, with diameters above 100 μm, is smaller than in the samples processed by lower numbers of rotations, as shown in Fig. 5.

A compositional EDX analysis of the selected area was performed in the form of maps, as presented in Fig. 6. It is apparent that the analysed zone contains both Al and Ti, where Al is the matrix and Ti occurs in the form of larger fragments as well as within the mixing zones with Al.

To analyse the grain refinement and mixing processes in the sample after 50 turns, a TEM/STEM analysis was conducted. In Fig. *7* representative STEM (a,b,c) and TEM (d,e) images of the 5-layered Al-Ti system processed by HPT for 50 turns are presented. Fig. 7a,b shows overall images of the sample in BF and HAADF modes, respectively. In the HAADF image there are bands enriched in Ti (bright), an Al matrix (dark grey) and mixing zones of Al-Ti (light grey). Mixing zones, in the form of bands, form a particular layered structure with alternately occurring zones of mixing placed inside an Al matrix with a width of less than ~70 nm, as presented in Fig. 7d,e. Grains inside the mixing zone, indicated by red arrows in Fig. 7d, have a size below 30 nm, while grains in the Al matrix are around 200 nm. Grains in the Al matrix (Fig. 7c,e) are distinguished by the presence of dislocations forming a cell structure, while grains in the mixing zone are in general free of any defects. Yellow arrows are used to mark another peculiarity of the microstructure where there are very thin layers with thicknesses of around 30 nm that are rich in Ti, that vertically subdivide the layers, as was described earlier for the Al-Mg system [34]. Those layers are probably a mixture of Al and Ti, generated during processing by high-pressure torsion. By contrast, the average grain sizes in the separate Al and Ti disks were measured as ∼700 and ∼100 nm, respectively, after processing by HPT for 10 turns.

Linear chemical analysis, as illustrated in Fig. 8, was performed on a cross-section through the Ti-enriched bands. The point scanning and the line profile revealed that the thin layers are composed of 75-86% of Al (red line) and 14-25% of Ti (green line), thereby indicating the formation of the Al_3Ti phase.

To confirm the formation of intermetallic phases inside the mixing zones, complementary SAED pattern analyses were performed, as presented in Fig. 9. The electron diffraction patterns confirmed the presence of intermetallic grains randomly distributed in the matrix, such as AlTi, Al_3Ti and $AlTi_3$. Strong diffraction rings for the (001) AlTi and (101) Al_3Ti phases can be observed in the inner part of the diffractogram. It is noted that the formation of such intermetallic phases is consistent with other reports on Al-Ti systems [35–38].

The phase compositions were also complemented by XRD analysis and the pattern for the sample after 50 turns is shown in Fig. 10. These patterns reveal a significant broadening of the

peaks due to the severe grain refinement. The patterns also confirm the presence of the Al and Ti phases and the formation of the AlTi, $AlTi_3$ and Al_3Ti phases with a strongest peak for the Al_3Ti phase.

3.2.Evaluation of mechanical properties

3.2.1. Microhardness

Microhardness measurements were performed as a first step to evaluate the mechanical properties of the hybrid material and for a comparison with the properties of the initial materials. The hardness distribution across the disk radius is presented in Fig. 11 a. where the hardness values in the initial state were 26 and 219 Hv for Al and Ti, respectively. After processing by HPT, the hardness in both samples underwent a significant increase with an average hardness across the disk of 51 Hv and 316 Hv for Al and Ti, respectively. In Al processed for 10 turns of HPT, the hardness across the disk was reasonably homogeneous but with slightly lower values in the central area than in the peripheral region so that an essentially saturation condition was observed. In the case of Ti, the hardness values were less homogeneous but without a strong dependence on the distance from the centre.

In all samples, the minimum hardness values were located near the disk center and the maximum in the peripheral region with a gradual rise across the disks. In the Al-Ti sample processed by 50 turns, an increase in hardness was observed compared to the HPT-processed Al. The minimum hardness values in the center of the disk were close to the level of ~60 Hv for the HPT-processed Al 1050 alloy, while on the edge of a disk the values were very high and even exceeded ~250 Hv at the edge. In the peripheral region of the sample processed for 50 turns the hardness values were reasonably homogenous, indicating an efficient mixing between Al and Ti.

The hardness distribution map for the sample after 50 turns is presented in Fig.11b and this confirms the observations made during the linear chemical analysis. It is readily apparent that the sample exhibits a gradual increase in hardness across the disk with the lowest hardness values near the centre and the highest, at close to ~300 Hv, in the peripheral region. The increase in hardness is gradual and confirms the occurrence of a gradual mixing between Al and Ti.

3.2.2. Nanoindentation

Nanoindentation was used to examine the micro/nano-mechanical response of the Al–Ti system processed by HPT. Nanoindentation tests were performed as a complementary procedure for evaluating the mechanical properties.

Fig. 12a shows representative load-penetration depth curves measured at the edges of the Al-Ti hybrid material, the Al-1050 alloy in the HPT-processed and as-received states and the HPT-processed CP-Ti. Each curve was obtained from a series of at least 20 measurements. A significant decrease in the maximum and final penetration depths is observed between the Al-Ti hybrid material and the Al-1050 alloy thereby indicating a strengthening of the material. The indentation plot of the Al-Ti hybrid material (red) resembles that of the HPT-processed titanium which suggests that the properties of the composite became closer to that of the HPT-processed Ti. As shown in Table 1, the hardness and Young´s modulus values of the Al-Ti hybrid material

are significantly higher than for the as-received and HPT-processed Al, with a Young´s modulus of 105 GPa (increase of 40% when compared to HPT-processed Al) and a hardness value of 3720 MPa (increase of 420% when compared to HPT-processed Al).

The ratio of H/E_r presented in Table 1 was measured as an indication of the wear resistance. As was shown in earlier reports [39,40], both hardness as well as the reciprocal value of elastic modulus have an influence on the wear resistance (higher H and lower E_r improve wear resitance). Therefore, the higher H/E_r ratio of the Al-Ti hybrid and HPT-processed Ti indicates a higher wear resistance than for the HPT-processed Al and as-received Al.

In Table 1 and Fig 12b information is given on the ratio of the elastic and plastic energies versus the total energy of deformation during nanoindentation. It is demonstrated that the contribution of elastic energy is higher for the Al-Ti hybrid and the HPT-processed Ti (23% and 26%, respectively) than for the as-received and HPT-processed Al (3% and 6%, respectively). The higher contribution of elastic energy in the total energy of deformation is an indication of a higher elastic recovery and therefore of the ability of a material to regain the initial shape after deformation. On the other hand, the contribution of plastic energy in the total energy of deformation (sometimes called "plasticity index") is an indication of the overall plasticity of the material. Therefore, the HPT-processed Al and the as-received Al show higher plasticity than the HPT-processed Ti and the Al-Ti hybrid.

Table 1 Values of Young´s modulus, hardness and energies of deformation

Sample	Young´s modulus (GPa)	Hardness (MPa)	H/E (wear resistance)	W_{elast}/W_{total}	W_{plast}/W_{total}
Al-Ti HPT	105±5	3720±346	0.035	0.23	0.77
Al 1050 HPT	81±2	714±12	0.009	0.06	0.94
Al 1050 as-received	79±1	449±15	0.006	0.03	0.97
Ti HPT	114±4	5330±528	0.047	0.26	0.74

4. Discussion

4.1. Unique microstructure formation in the Al-Ti hybrid system

The results from this investigation demonstrate that the HPT technique has a potential for producing a bonding of dissimilar bulk metals when suitable processing parameters are applied. Earlier studies described the potential for using HPT as a technique for the synthesis of hybrid materials for systems such as Al-Mg [20,21], Al-Cu [18,22–24], Cu-Sn [41], steel-vanadium [42] and Al-Ti [31]. HPT-processed hybrid systems can be characterized by a unique layered microstructure [20,42] with significant grain refinement [21,42] and the formation of intermetallic phases [18,20] as well as enhanced mechanical properties [20,42]. However, it should be noted that the microstructure of processed Al-Ti disks is strongly influenced by the processing parameters. Depending on the numbers of HPT turns, the disks may contain a variety of microstructural features such as bent, cracked and fragmented parts of the Ti disks or vortex like structures and lamellar systems [43,44] which determine the potential of the hybrid materials to exhibit superior mechanical properties [45–49]. This suggests that a certain physical mechanism governs the transformation of the structural components inside the sample

at the stage of transition from a wavy laminar flow to chaotic mixing of the components. For this reason it is crucial to determine the method for creating these structures.

During the HPT of laminates, the hard layers inhibit the shear in the soft layers. This leads to a strain gradient. This is confirmed by experiments showing that grain refinement with the formation of high-angle grain boundaries is more pronounced and occurs more quickly in softer alloys than in harder ones [50]. At the interface, the hard layer constrains the deformation of the soft one, which means that the soft layer is compressed and the hard one is under tension. Accordingly, buckling of their interface towards the hard layer occurs. At certain point periodic constrictions appear in the titanium layers leading to their fragmentation. The SEM and μCT investigations (Figs 2 and 4) confirm that in the initial stages of deformation, corresponding to low numbers of revolutions, when the shear forces exceed a critical level the harder Ti phase is refined continuously by elongation, repeated bending or necking and by a fragmentation into smaller elements [51]. Fig. 13 presents some structural images illustrating the model of further deformation of these Ti fragments. With increasing numbers of HPT turns, the overall hardness of the hybrid increases which leads to a strong shear localization. Due to this, small fragments of Ti are torn off from the Ti disk (Fig. 13a,b) and they pass into the Al matrix. Thereafter, these Ti fragments undergo further intense deformation, forming a vortex-like structure consisting of very thin Ti layers alternately arranged within the Al matrix, as shown in Fig. 13b,c. At a certain point, severely refined fragments of Ti are mixed with Al forming a lamellar structure, as illustrated in Fig. 13c. As a result, after 50 HPT turns almost a full mixing of elements is achieved in the edge regions of the disks. The final microstructure after 50 HPT turns is a composite containing an Al-rich matrix with a grain size of ∼200 nm and fine Ti-rich layers with a size of about ∼30 nm which are dispersed evenly within the matrix.

Moreover, it was also shown that intermetallic Al-Ti phases were generated within these lamellar structures. The formation of intermetallic phases is possible due to enhanced atomic reactions during HPT processing which are influenced by the increased density of lattice defects (vacancies, dislocations and grain boundaries) and the reduction in the atomic diffusion distance due to microstructural refinement [18,52]. As a consequence of the grain refinement, the atomic diffusion paths are shortened and this enables solid-state reactions and the formation of intermetallic phases as confirmed through the EDX mapping and SAED in Fig. 8 and Fig. 9, respectively. Such a microstructure achieved by HPT processing leads to very significant improvements in the mechanical properties. The present hybrid material exhibits extraordinary mechanical properties measured by the microhardness (Hv of 300) and nanoindentation tests (H ~3700 MPa and Young modulus of 105 GPa).

4.2.Saturation shift in the hybrid materials

Although severe plastic deformation methods are widely recognized as fabrication techniques for ultrafine-grained and even nanocrystalline materials, it is also well known that obtaining a true nanocrystalline structure, especially in pure metals, is very difficult. This is due to a saturation effect which can be explained as a certain level of accumulated strain above which it is impossible to achieve further microstructural refinement and strengthening [53,54]. To date, several techniques were implemented in order to overcome the saturation effect and thereby to obtain a more refined structure and better mechanical performances of the SPD-processed materials. One of these techniques is the use of a combination of two or more different SPD methods to activate more slip systems, such as hydrostatic extrusion followed by HPT [53] or ECAP followed by HPT [54–57]. It was demonstrated that a combination of two

SPD methods provides an advantage in grain refinement when compared with processing only by HPT.

In this study, an alternative approach was proposed to overcome the saturation effect through the fabrication of hybrid materials by subjecting a set of dissimilar metal disks to HPT processing. The matrix material used in this study was a commercial purity aluminium alloy Al-1050 which exhibits a saturation effect after processing through 5 or more HPT turns at 298 K [58–60]. To study the saturation effect in the hybrid Al-Ti, the experimental microhardness points from Fig.12 were plotted in Fig.14 against the equivalent strain and the experimental data were supplemented with the datum points for the initial Al and Ti metals after 10 HPT turns. First of all it should be mentioned that Eq. 1 can be used only to give a very rough estimate the equivalent strain in hybrid materials. It does not take into account the stress concentration on the interfaces between the soft Al and hard Ti phases, interactions with intermetallic phases or shearing instabilities in the turbulent flow model [12]. The procedure for correctly calculating the equivalent strain of hybrid materials seems to be the next challenge for researchers

The datum points for the initial materials are in reasonable agreement and fall around the solid line. In the early stages of HPT, the hardness values for Al and Ti rise very rapidly with the accumulating strain but ultimately there is no significant further increase at equivalent strains above ~20 and ~70 for these two materials, respectively, and thereafter the microhardness values become essentially saturated at Hv ≈ 51 and Hv ≈ 350, respectively. Nevertheless, the Al-Ti hybrid system processed under 50 HPT turns behaves differently. In the first stages of deformation (equivalent strains < 300-400) the hardness values are essentially uniform (~50 Hv units) with only a few points of higher hardness values (100-150 Hv). However, a further increase in the strain produces a successive increase in hardness (above 300 Hv), without the occurrence of any saturation effect. The nanoindentation study not only confirmed the large increase of hardness, but also of the H/E_r ratio in the Al-Ti hybrid system, indicating much higher wear resistance when compared to the HPT-processed Al 1050. This unusual behaviour can be explained by the formation of a solid solution between the Al and Ti phases. For low strains, and in the mid-sections of the disks, there is no apparent mixing of materials (Figs 2 and 4). This means that the only phenomenon occurring in the microstructure is grain refinement which is so intense after 50 HPT turns that it induces saturation in the Al and Ti phases. In the edge regions where the strain is higher the microhardness increases due to the mixing of the Al and Ti elements. This notable enhancement in the strain hardenability appears to be due to the combination of multiple strengthening mechanisms, including solid solution strengthening which has a strong impact on the minimum grain size and Hall-Petch strengthening [61] . However, the observed strain hardening in the present Al-Ti hybrids is mainly attributed *to in-situ* phase transformations of Al to the hard AlTi, $AlTi_3$ and Al_3Ti phases (Figs 9 and 10) [35,36]. A similar hardening effect was also reported earlier for other hybrid systems synthesized by HPT such as the Zn–Mg system [26] where the hardness after HPT was eight times higher than for the initial material, the Al–Cu system [24] where the hardness was five times higher and the Al–Mg system [20,61] where the hardness three times higher.

The results presented in this study on the mechanical bonding of dissimilar metals by HPT demonstrates that the fabrication of hybrid materials may be a simple and readily available solution for overcoming, or at least shifting, the saturation effect by means of the applied strain while continuing to achieve enhanced grain refinement and superior mechanical performances in the as-produced materials.

5. Conclusions

- Al-Ti hybrid materials were synthesised using quasi-constrained HPT processing under 6.0 GPa and 1 rpm for 10, 20, 30, 40 and 50 turns. The microstructures and mechanical properties evolution were investigated by SEM, TEM/STEM, SAED, MicroCT, XRD, Vickers microhardness and nano-indentation testing.
- A relatively homogeneous lamellar microstructure, consisting of an ultrafine-grained (~200 nm) Al matrix and nanoscale (~30 nm) Ti rich layers, was formed at the disk periphery after 50 HPT turns.
- After 50 turns of HPT processing, the Al-Ti hybrid material exhibited remarkably improved hardness and Young's modulus by comparison with the initial commercial purity Al and Ti. The average Vickers microhardness value was ~300 Hv and the Young's modulus measured in nanoindentation was ~105 GPa.
- HPT promotes the solid-state reaction of Al and Ti elements so that there is the formation of AlTi, Al_3Ti and $AlTi_3$ phases as well as a dissolution of Al and Ti components in each matrix.
- An investigation of the strain hardening capacity revealed that the Al-Ti hybrid system follows a two-regime behaviour during HPT processing. The first regime, up to an equivalent strain of ~400, indicates regions with no mixing of materials and limited strain hardening. The second region, above an equivalent strain of ~400, exhibits exceptional strain hardening due to intense grain refinement, solid-state reactions and the formation of intermetallic phases.
- The results demonstrate the potential for using HPT processing at room temperature to create advanced microstructures and excellent mechanical properties that are not generally achievable through other processing routes.

Acknowledgments

This research was funded by **POB Technologie Materiałowe** of Warsaw University of Technology within the Excellence Initiative: Research University (IDUB) programme. TGL and YH were supported by the European Research Council under ERC Grant Agreement No. 267464-SPDMETALS. One of the authors acknowledges funding from the Generalitat de Catalunya (project no. 2017-SGR-0292).

P. Bazarnik: Conceptualization, Methodology, Investigation, Data curation, Writing – original draft, Project administration, Funding acquisition.

A. Bartkowska: Conceptualization, Methodology, Validation, Writing – review & editing.

Y. Huang: Processing, investigation

K. Szlązak: Investigation, Data curation, Visualization

B. Adamczyk-Cieślak: Investigation, Data curation, Visualization

J. Sort: Validation, Writing – review & editing

M. Lewandowska: Conceptualization, Writing – review & editing

T.G. Langdon: Conceptualization, Supervision, Writing – review & editing

Bibliography

[1] A.P. Zhilyaev, T.G. Langdon, Using high-pressure torsion for metal processing: Fundamentals and applications, Progress in Materials Science 53 (2008) 893–979. https://doi.org/10.1016/j.pmatsci.2008.03.002.

[2] R.Z. Valiev, Producing bulk nanostructured metals and alloys by severe plastic deformation (SPD), Nanostructured Metals and Alloys, Woodhead Publishing Series in Metals and Surface Engineering (2011) 3–39. https://doi.org/10.1533/9780857091123.1.3.

[3] T.G. Langdon, Twenty-five years of ultrafine-grained materials: Achieving exceptional properties through grain refinement, Acta Materialia 61 (2013) 7035–7059. https://www.sciencedirect.com/science/article/pii/S1359645413006149

[4] R.Z. Valiev, Y. V. Ivanisenko, E.F. Rauch, B. Baudelet, Structure and deformaton behaviour of Armco iron subjected to severe plastic deformation, Acta Materialia 44 (1996) 4705–4712. https://doi.org/10.1016/S1359-6454(96)00156-5.

[5] M. Kawasaki, B. Ahn, T.G. Langdon, Significance of strain reversals in a two-phase alloy processed by high-pressure torsion, Materials Science and Engineering: A 527 (2010) 7008–7016. https://doi.org/10.1016/J.MSEA.2010.07.090.

[6] M. Kawasaki, H.J. Lee, B. Ahn, A.P. Zhilyaev, T.G. Langdon, Evolution of hardness in ultrafine-grained metals processed by high-pressure torsion, Journal of Materials Research and Technology 3 (2014) 311–318. https://doi.org/10.1016/j.jmrt.2014.06.002.

[7] M. Kawasaki, Different models of hardness evolution in ultrafine-grained materials processed by high-pressure torsion, Journal of Materials Science 49 (2013) 18–34. https://doi.org/10.1007/S10853-013-7687-9.

[8] M. Kawasaki, R.B. Figueiredo, T.G. Langdon, An investigation of hardness homogeneity throughout disks processed by high-pressure torsion, Acta Materialia 59 (2011) 308-316. https://doi.org/10.1016/j.actamat.2010.09.034.

[9] A. Loucif, R.B. Figueiredo, T. Baudin, F. Brisset, R. Chemam, T.G. Langdon, Ultrafine grains and the Hall-Petch relationship in an Al-Mg-Si alloy processed by high-pressure torsion, Materials Science and Engineering A 532 (2012) 139–145. https://doi.org/10.1016/j.msea.2011.10.074.

[10] C. Xu, Z. Horita, T.G. Langdon, The evolution of homogeneity in processing by high-pressure torsion, Acta Materialia 55 (2007) 203–212. https://doi.org/10.1016/j.actamat.2006.07.029.

[11] T. Miyazaki, D. Terada, Y. Miyajima, C. Suryanarayana, R. Murao, Y. Yokoyama, K. Sugiyama, M. Umemoto, Y. Todaka, N. Tsuji, Synthesis of non-equilibrium phases in immiscible metals mechanically mixed by high pressure

torsion, Journal of Materials Science 46 (2011) 4296–4301. https://doi.org/10.1007/s10853-010-5240-7.

[12] R. Kulagin, Y. Beygelzimer, Y. Ivanisenko, A. Mazilkin, B. Straumal, H. Hahn, Instabilities of interfaces between dissimilar metals induced by high pressure torsion, Materials Letters 222 (2018) 172–175. https://doi.org/10.1016/j.matlet.2018.03.200.

[13] M.M. Castro, S. Sabbaghianrad, P.H.R. Pereira, E.M. Mazzer, A. Isaac, T.G. Langdon, R.B. Figueiredo, A magnesium-aluminium composite produced by high-pressure torsion, Journal of Alloys and Compounds 804 (2019) 421–426. https://doi.org/10.1016/j.jallcom.2019.07.007.

[14] J.K. Han, D.K. Han, G.Y. Liang, J. il Jang, T.G. Langdon, M. Kawasaki, Direct bonding of aluminum–copper metals through high-pressure torsion processing, Advanced Engineering Materials 20 (2018) 1800642. https://doi.org/10.1002/adem.201800642.

[15] J.K. Han, J. il Jang, T.G. Langdon, M. Kawasaki, Bulk-state reactions and improving the mechanical properties of metals through high-pressure torsion, Materials Transactions 60 (2019) 1131–1138. https://doi.org/10.2320/matertrans.MF201908.

[16] J.-K. Han, T. Herndon, J. Jang, T.G. Langdon, M. Kawasaki, Synthesis of hybrid nanocrystalline alloys by mechanical bonding through high-pressure torsion, Advanced Engineering Materials 22 (2020) 1901289. https://doi.org/10.1002/adem.201901289.

[17] M. Kawasaki, T.G. Langdon, Using severe plastic deformation to fabricate strong metal matrix composites, Materials Research 20 (2017) 46–52. https://doi.org/10.1590/1980-5373-MR-2017-0218.

[18] K. Oh-Ishi, K. Edalati, H.S. Kim, K. Hono, Z. Horita, High-pressure torsion for enhanced atomic diffusion and promoting solid-state reactions in the aluminum-copper system, Acta Materialia. 61 (2013) 3482–3489. https://doi.org/10.1016/j.actamat.2013.02.042.

[19] O. Bouaziz, H.S. Kim, Y. Estrin, Architecturing of metal-based composites with concurrent nanostructuring: A new paradigm of materials design, Advanced Engineering Materials. 15 (2013) 336–340. https://doi.org/10.1002/adem.201200261.

[20] B. Ahn, A.P. Zhilyaev, H.-J. Lee, M. Kawasaki, T.G. Langdon, Rapid synthesis of an extra hard metal matrix nanocomposite at ambient temperature, Materials Science and Engineering: A 635 (2015) 109-117. https://doi.org/10.1016/j.msea.2015.03.042.

[21] B. Ahn, H.-J. Lee, I.-C. Choi, M. Kawasaki, J.-I. Jang, T.G. Langdon, Micro-mechanical behavior of an exceptionally strong metal matrix nanocomposite processed by high-pressure torsion, Advanced Engineering Materials 18 (2016) 1001–1008. https://doi.org/10.1002/adem.201500520.

[22] V.N. Danilenko, S.N. Sergeev, J.A. Baimova, G.F. Korznikova, K.S. Nazarov, R.K. Khisamov, A.M. Glezer, R.R. Mulyukov, An approach for fabrication of Al-Cu composite by high pressure torsion, Materials Letters 236 (2019) 51–55. https://doi.org/10.1016/j.matlet.2018.09.158.

[23] G.F. Korznikova, K.S. Nazarov, R.K. Khisamov, S.N. Sergeev, R.U. Shayachmetov, G.R. Khalikova, J.A. Baimova, A.M. Glezer, R.R. Mulyukov, Intermetallic growth kinetics and microstructure evolution in Al-Cu-Al metal-matrix composite processed by high pressure torsion, Materials Letters 253 (2019) 412–415. https://doi.org/10.1016/j.matlet.2019.07.124.

[24] P. Bazarnik, A. Bartkowska, B. Romelczyk-Baishya, B. Adamczyk-Cieślak, J. Dai, Y. Huang, M. Lewandowska, T.G. Langdon, Superior strength of tri-layered Al–Cu–Al nano-composites processed by high-pressure torsion, Journal of Alloys and Compounds 846 (2020) 156380. https://doi.org/10.1016/j.jallcom.2020.156380.

[25] T. Mousavi, J. Dai, P. Bazarnik, P.H.R. Pereira, Y. Huang, M. Lewandowska, T.G. Langdon, Fabrication and characterization of nanostructured immiscible Cu–Ta alloys processed by high-pressure torsion, Journal of Alloys and Compounds 832 (2020) 155007. https://doi.org/10.1016/j.jallcom.2020.155007.

[26] D. Hernández-Escobar, J. Marcus, J.K. Han, R.R. Unocic, M. Kawasaki, C.J. Boehlert, Effect of post-deformation annealing on the microstructure and micro-mechanical behavior of Zn–Mg hybrids processed by High-Pressure Torsion, Materials Science and Engineering A 771 (2020) 138578. https://doi.org/10.1016/j.msea.2019.138578.

[27] D. Hernández-Escobar, Z.U. Rahman, H. Yilmazer, M.V. Kawasaki, C.J. Boehlert, Microstructural evolution and intermetallic formation in Zn-Mg hybrids processed by high-pressure torsion, Philosophical Magazine. 99 (2019) 557-584. https://doi.org/10.1080/14786435.2018.1546962.

[28] S.O. Rogachev, V.M. Khatkevich, S.A. Nikulin, M. Ignateva, A.A. Gromov, High thermally stable multi-layer steel/vanadium alloy hybrid material obtained by high-pressure torsion, Materials Letters 255 (2019) 126527. https://doi.org/10.1016/j.matlet.2019.126527.

[29] A. Korneva, B. Straumal, R. Chulist, A. Kilmametov, P. Bała, G. Cios, N. Schell, P. Zięba, Grain refinement of intermetallic compounds in the Cu–Sn system under high pressure torsion, Materials Letters 179 (2016) 12-15. https://doi.org/10.1016/j.matlet.2016.05.059.

[30] D. Luo, T. Huminiuc, Y. Huang, T. Polcar, T.G. Langdon, The fabrication of high strength Zr/Nb nanocomposites using high-pressure torsion, Materials Science and Engineering A 790 (2020) 139693. https://doi.org/10.1016/j.msea.2020.139693.

[31] A. Bartkowska, P. Bazarnik, Y. Huang, M. Lewandowska, T.G. Langdon, Using high-pressure torsion to fabricate an Al–Ti hybrid system with exceptional

mechanical properties, Materials Science and Engineering A 799 (2021) 140114. https://doi.org/10.1016/j.msea.2020.140114.

[32] R.B. Figueiredo, P.H.R. Pereira, M.T.P. Aguilar, P.R. Cetlin, T.G. Langdon, Using finite element modeling to examine the temperature distribution in quasi-constrained high-pressure torsion, Acta Materialia 60 (2012) 3190–3198. https://doi.org/10.1016/J.ACTAMAT.2012.02.027.

[33] W.C. Oliver, G.M. Pharr, An improved technique for determining hardness and elastic modulus using load and displacement sensing indentation experiments, Journal of Materials Research 7 (1992) 1564–1583. https://doi.org/10.1557/jmr.1992.1564.

[34] M. Kawasaki, J.K. Han, D.H. Lee, J. Il Jang, T.G. Langdon, Fabrication of nanocomposites through diffusion bonding under high-pressure torsion, Journal of Materials Research 33 (2018) 2700–2710. https://doi.org/10.1557/jmr.2018.205.

[35] Z. Lee, R. Rodriguez, R.W. Hayes, E.J. Lavernia, S.R. Nutt, Microstructural evolution and deformation of cryomilled nanocrystalline Al-Ti-Cu alloy, Metallurgical and Materials Transactions A: Physical Metallurgy and Materials Science 34 (2003) 1473–1481. https://doi.org/10.1007/s11661-003-0259-x.

[36] K. Edalati, S. Toh, H. Iwaoka, M. Watanabe, Z. Horita, D. Kashioka, K. Kishida, H. Inui, Ultrahigh strength and high plasticity in TiAl intermetallics with bimodal grain structure and nanotwins, Scripta Materialia 67 (2012) 814–817. https://doi.org/10.1016/j.scriptamat.2012.07.030.

[37] P. Bazarnik, B. Adamczyk-Cieślak, A. Gałka, B. Płonka, L. Snieżek, M. Cantoni, M. Lewandowska, Mechanical and microstructural characteristics of Ti6Al4V/AA2519 and Ti6Al4V/AA1050/AA2519 laminates manufactured by explosive welding, Materials and Design. 111 (2016) 146–157. https://doi.org/10.1016/j.matdes.2016.08.088.

[38] D.M. Fronczek, R. Chulist, L. Litynska-Dobrzynska, G.A. Lopez, A. Wierzbicka-Miernik, N. Schell, Z. Szulc, J. Wojewoda-Budka, Microstructural and phase composition differences across the interfaces in Al/Ti/Al explosively welded clads, Metallurgical and Materials Transactions A: Physical Metallurgy and Materials Science 48 (2017) 4154–4165. https://doi.org/10.1007/s11661-017-4169-8.

[39] A. Leyland, A. Matthews, On the significance of the H/E ratio in wear control: A nanocomposite coating approach to optimised tribological behaviour, Wear 246 (2000) 1–11. https://doi.org/10.1016/S0043-1648(00)00488-9.

[40] E. Pellicer, S. Pané, K.M. Sivaraman, O. Ergeneman, S. Suriñach, M.D. Baró, B.J. Nelson, J. Sort, Effects of the anion in glycine-containing electrolytes on the mechanical properties of electrodeposited Co-Ni films, Materials Chemistry and Physics 130 (2011) 1380–1386. https://doi.org/10.1016/j.matchemphys.2011.09.032.

[41] A. Korneva, B. Straumal, A. Kilmametov, L. Lityńska-Dobrzyńska, G. Cios, P. Bała, P. Zięba, Effect of high pressure torsion on microstructure of Cu-Sn alloys with different content of Hume Rothery phase, Materials Characterization 118 (2016) 411–416. https://doi.org/10.1016/j.matchar.2016.06.019.

[42] S.O. Rogachev, R.V. Sundeev, V.M. Khatkevich, Evolution of the structure and strength of steel/vanadium alloy/steel hybrid material during severe plastic deformation, Materials Letters 173 (2016) 123–126. https://doi.org/10.1016/j.matlet.2016.03.044.

[43] R. Kulagin, Y. Beygelzimer, A. Bachmaier, R. Pippan, Y. Estrin, Benefits of pattern formation by severe plastic deformation, Applied Materials Today. 15 (2019) 236–241. https://doi.org/10.1016/J.APMT.2019.02.007.

[44] Y. Beygelzimer, Y. Estrin, A. Mazilkin, T. Scherer, B. Baretzky, H. Hahn, R. Kulagin, Quantifying solid-state mechanical mixing by high-pressure torsion, Journal of Alloys and Compounds 878 (2021) 160419. https://doi.org/10.1016/j.jallcom.2021.160419.

[45] K. Lu, Making strong nanomaterials ductile with gradients: Microstructures that increase metal crystallite size from nanoscale with surface depth are both strong and ductile, Science 345 (2014) 1455–1456. https://doi.org/10.1126/science.1255940.

[46] T.H. Fang, W.L. Li, N.R. Tao, K. Lu, Revealing extraordinary intrinsic tensile plasticity in gradient nano-grained copper, Science 331 (2011) 1587–1590. https://doi.org/10.1126/science.1200177.

[47] X. Wu, P. Jiang, L. Chen, F. Yuan, Y.T. Zhu, Extraordinary strain hardening by gradient structure, Proceedings of the National Academy of Sciences of the United States of America 111 (2014) 7197–7201. https://doi.org/10.1073/pnas.1324069111.

[48] X.L. Wu, P. Jiang, L. Chen, J.F. Zhang, F.P. Yuan, Y.T. Zhu, Synergetic strengthening by gradient structure, Materials Research Letters 2 (2014) 185–191. https://doi.org/10.1080/21663831.2014.935821.

[49] X. Wu, Y. Zhu, K. Lu, Ductility and strain hardening in gradient and lamellar structured materials, Scripta Materialia 186 (2020) 321–325. https://doi.org/10.1016/j.scriptamat.2020.05.025.

[50] D. Rahmatabadi, A. Shahmirzaloo, M. Farahani, M. Tayyebi, R. Hashemi, Characterizing the elastic and plastic properties of the multilayered Al/Brass composite produced by ARB using DIC, Materials Science and Engineering A 753 (2019) 70–78. https://doi.org/10.1016/j.msea.2019.03.002.

[51] K.S. Kormout, R. Pippan, A. Bachmaier, Deformation-induced supersaturation in immiscible material systems during high-pressure torsion, Advanced Engineering Materials. 19 (2017) 1600675. https://doi.org/10.1002/adem.201600675.

[52] K. Edalati, S. Toh, M. Watanabe, Z. Horita, In situ production of bulk intermetallic-based nanocomposites and nanostructured intermetallics by high-

pressure torsion, Scripta Materialia 66 (2012) 386–389. https://doi.org/10.1016/j.scriptamat.2011.11.039.

[53] P. Bazarnik, Y. Huang, M. Lewandowska, T.G. Langdon, Enhanced grain refinement and microhardness by hybrid processing using hydrostatic extrusion and high-pressure torsion, Materials Science and Engineering: A 712 (2018) 513–520. https://doi.org/10.1016/j.msea.2017.12.007.

[54] V.V. Popov, E.N. Popova, A.V. Stolbovskiy, Nanostructuring Nb by various techniques of severe plastic deformation, Materials Science and Engineering A 539 (2012) 22–29. https://doi.org/10.1016/j.msea.2011.12.082.

[55] S. Sabbaghianrad, T.G. Langdon, A critical evaluation of the processing of an aluminum 7075 alloy using a combination of ECAP and HPT, Materials Science and Engineering A 596 (2014) 52–58. https://doi.org/10.1016/j.msea.2013.12.034.

[56] S. Sabbaghianrad, T.G. Langdon, An evaluation of the saturation hardness in an ultrafine-grained aluminum 7075 alloy processed using different techniques, Journal of Materials Science 50 (2015) 4357–4365. https://doi.org/10.1007/S10853-015-8989-X.

[57] S. Sabbaghianrad, S.A. Torbati-Sarraf, T.G. Langdon, An investigation of the limits of grain refinement after processing by a combination of severe plastic deformation techniques: A comparison of Al and Mg alloys, Materials Science and Engineering A 712 (2018) 373–379. https://doi.org/10.1016/j.msea.2017.11.090.

[58] Y. Huang, P. Bazarnik, D. Wan, D. Luo, P.H.R. Pereira, M. Lewandowska, J. Yao, B.E. Hayden, T.G. Langdon, The fabrication of graphene-reinforced Al-based nanocomposites using high-pressure torsion, Acta Materialia 164 (2019) 499–511. https://doi.org/10.1016/j.actamat.2018.10.060.

[59] S.N. Alhajeri, M. Kawasaki, N. Gao, T.G. Langdon, The evolution of homogeneity during processing of aluminium alloys by HPT, Materials Science Forum 667–669 (2011) 277–282. https://doi.org/10.4028/www.scientific.net/MSF.667-669.277.

[60] M. Kawasaki, S.N. Alhajeri, C. Xu, T.G. Langdon, The development of hardness homogeneity in pure aluminum and aluminum alloy disks processed by high-pressure torsion, Materials Science and Engineering A 529 (2011) 345–351. https://doi.org/10.1016/j.msea.2011.09.039.

[61] J.-K. Han, H.-J. Lee, J. Jang, M. Kawasaki, T.G. Langdon, Micro-mechanical and tribological properties of aluminum-magnesium nanocomposites processed by high-pressure torsion, Materials Science and Engineering: A 684 (2017) 318–327. https://doi.org/10.1016/j.msea.2016.12.067.

List of Figures:

Fig. 1 LM images of Al-Ti samples after various numbers of HPT rotations

Fig. 2 MicroCT 3D-reconstruction of Al-Ti composite after 10 HPT turns. Perspective view a), cross-section view b) and disc plane view c). Scan of a quarter of HPT disk where Ti plates (marked as red) are severly bent and fragmented.

Fig. 3 MicroCT 3D-reconstruction of Al-Ti composite after 50 HPT turns. Perspective view a), cross-section view b) and disc plane view c). Scan of a small region of HPT disk, mid-section of the disk, showing strong fragmentation of Ti phase (marked as red) and its uniform distribution in the Al matrix.

Fig. 4 Selected SEM images of the 5-layered system processed by HPT for: a) 10 turns, b and c) 20 turns. Red arrows indicate areas of delaminations and discontinuities.

Fig. 5 SEM images of the Al-Ti sample processed for 50 turns.

Fig. 6 EDX maps of the Al-Ti sample processed for 50 turns

Fig. 7 Selected TEM and STEM images of the sample processed for 50 turns.

Fig. 8 EDX linear analysis through the mixing layer, where Al is represented by the red line and Ti by the green line.

Fig. 9 SAED pattern showing presence of several intermetallic phases from the Al-Ti system

Fig. 10 XRD pattern of hybrid Al-Ti processed for 50 turns

Fig. 11 a) Microhardness distribution along the sample radius, b) Microhardness distribution across the disk in the Al-Ti sample processed for 50 turns

Fig. 12 a) Representative nanoindentation curves of Al-Ti hybrid material processed for 50 turns (red), Al-1050 processed for 10 turns (pink), Al 1050 in as-received state (blue) and Ti processed for 10 turns (green) and b) Reduced Young´s modulus and hardness of as-received and HPT-processed materials

Fig. 13 Exemplary SEM images of the Al/Ti interfaces after HPT deformation

Fig. 14 Hardness as a function of accumulated strain in the Al-Ti hybrid material processed for 50 turns. HPT-processed Al-1050 and CP-Ti are added as a reference

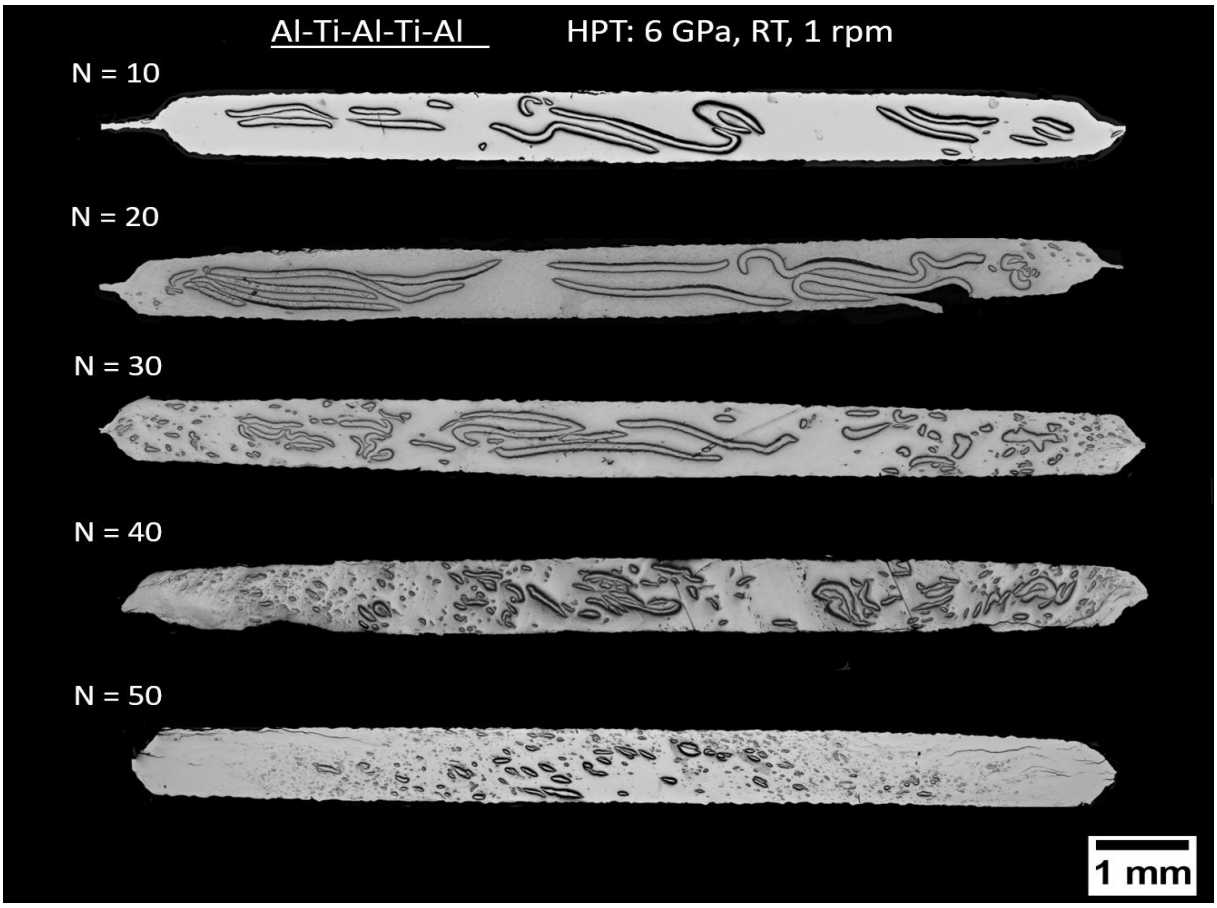

Fig. 1 LM images of Al-Ti samples after various numbers of HPT rotations

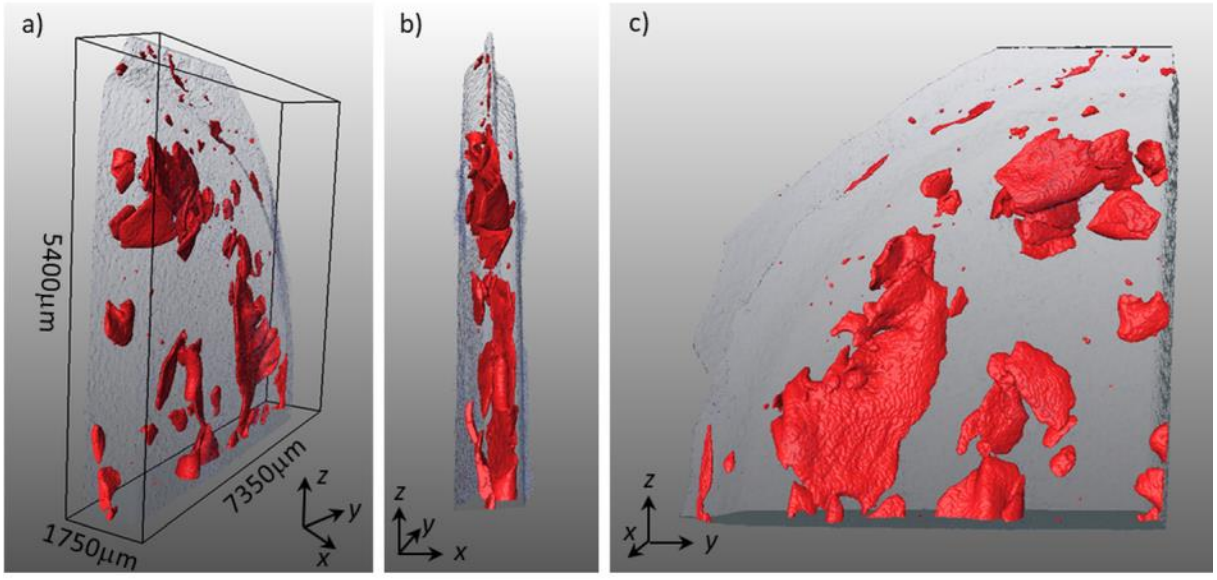

Fig. 2 MicroCT 3D-reconstruction of Al-Ti composite after 10 HPT turns. Scan of a quarter of HPT disk where Ti plates (marked as red) are severely bent and fragmented.

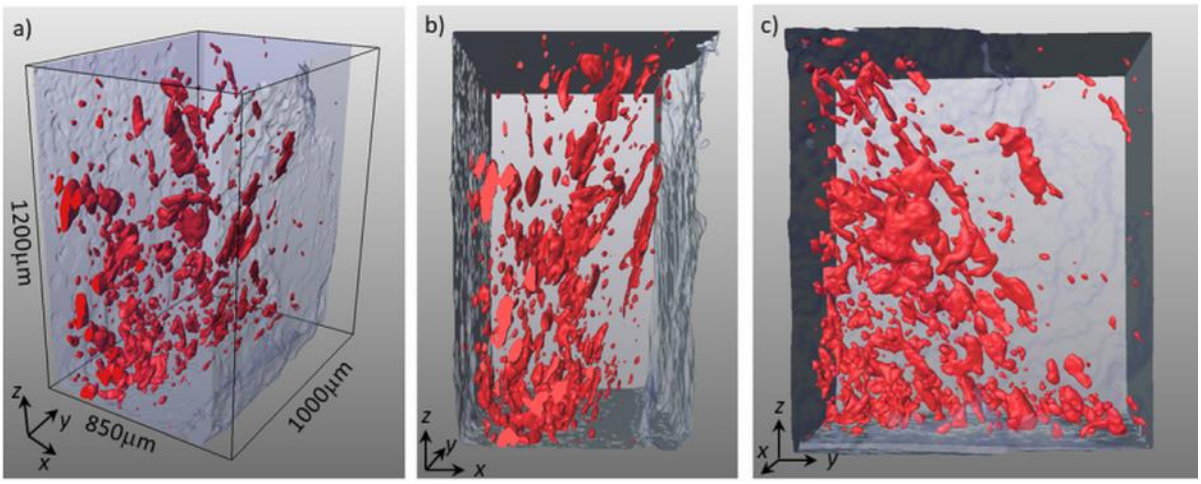

Fig. 3 MicroCT 3D-reconstruction of Al-Ti composite after 50 HPT turns. Scan of a small region of HPT disk, mid-section of the disk, showing strong fragmentation of Ti phase (marked as red) and its uniform distribution in the Al matrix.

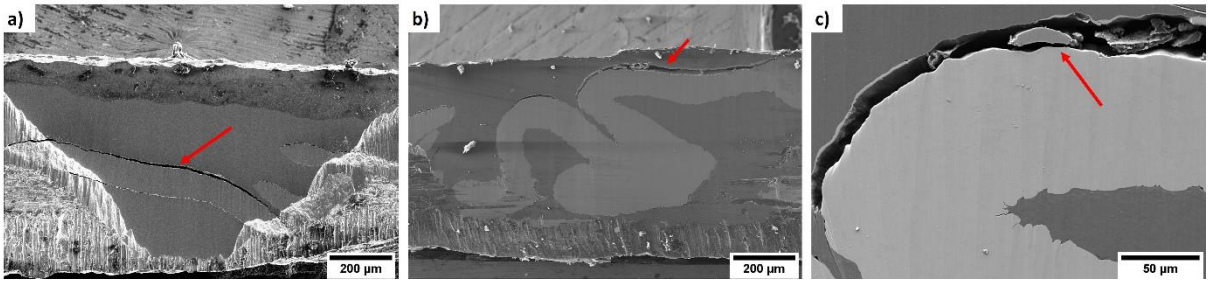

Fig. 4 Selected SEM images of the 5-layered system processed by HPT for: a) 10 turns, b and c) 20 turns. Red arrows indicate areas of delaminations and discontinuities.

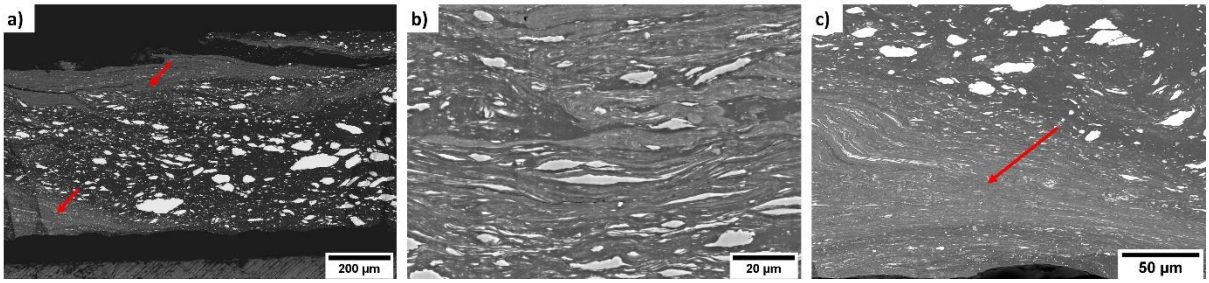

Fig. 5 SEM images of the Al-Ti sample processed for 50 turns.

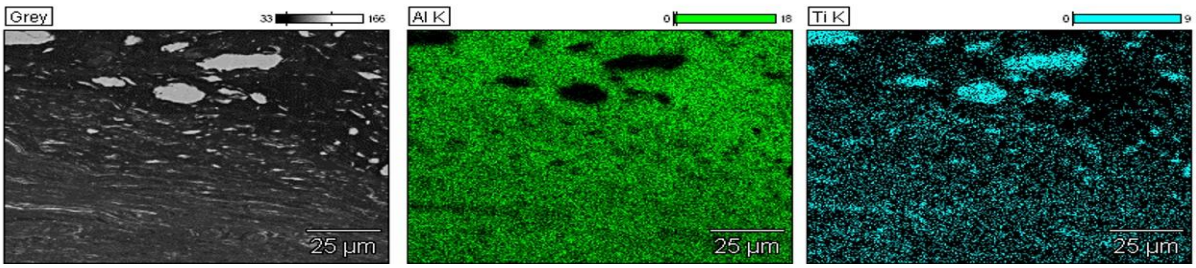

Fig. 6 EDX maps of the Al-Ti sample processed for 50 turns

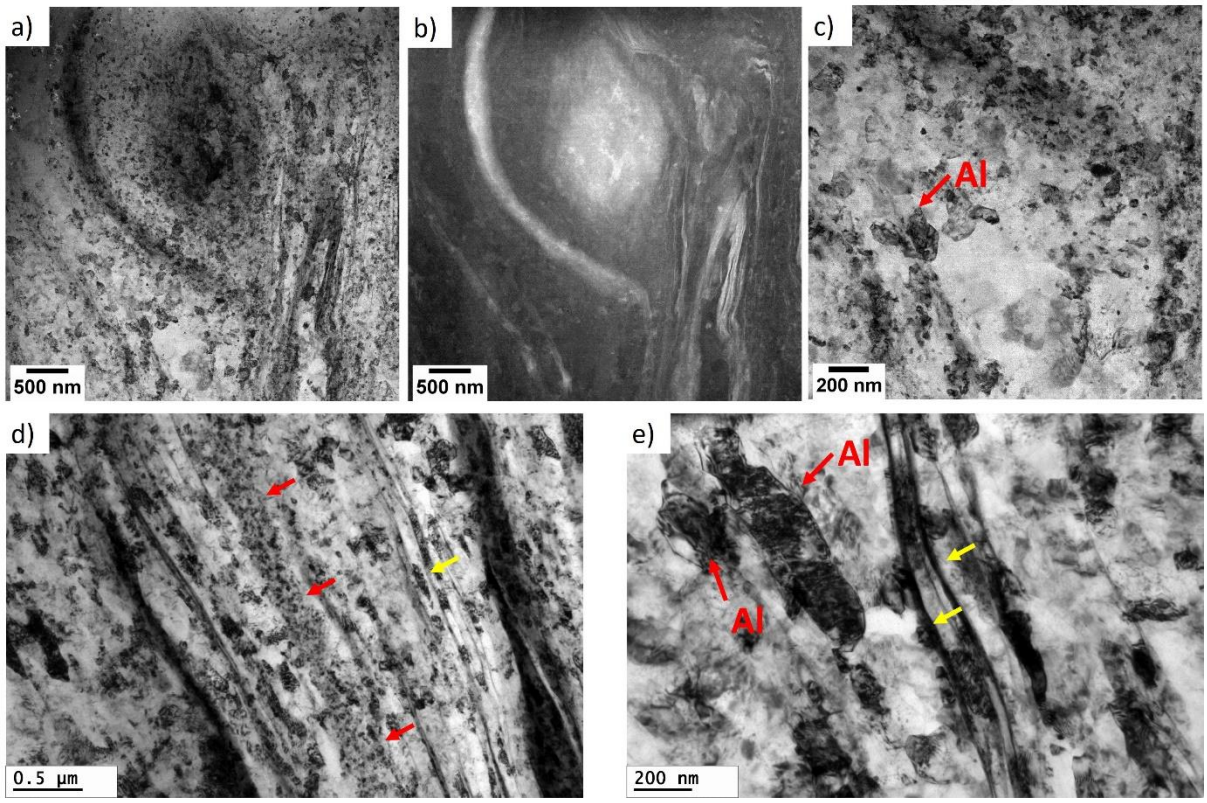

Fig. 7 Selected TEM and STEM images of the sample processed for 50 turns.

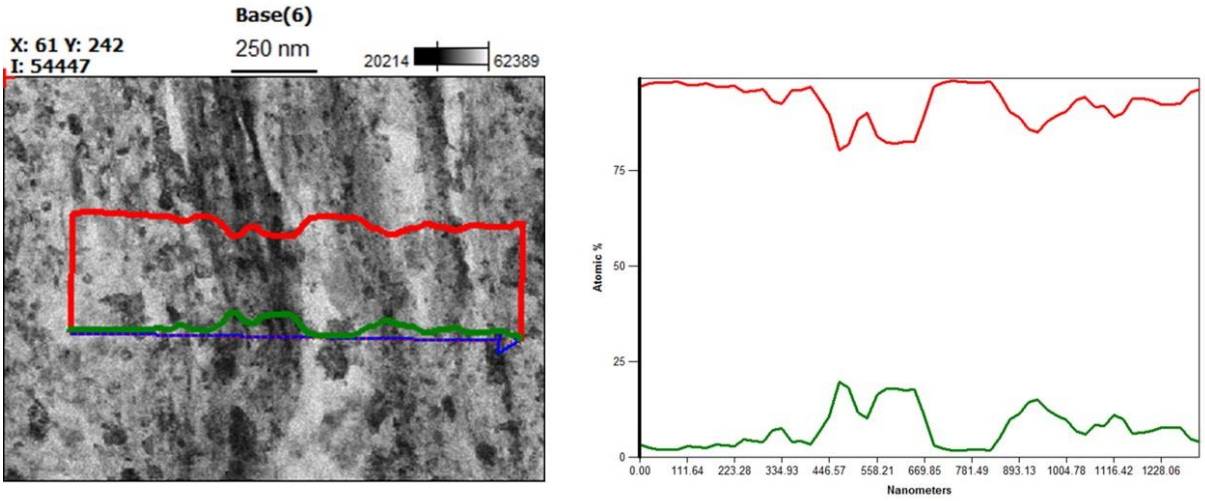

Fig. 8 EDX linear analysis through the mixing layer, where Al is represented by the red line and Ti by the green line.

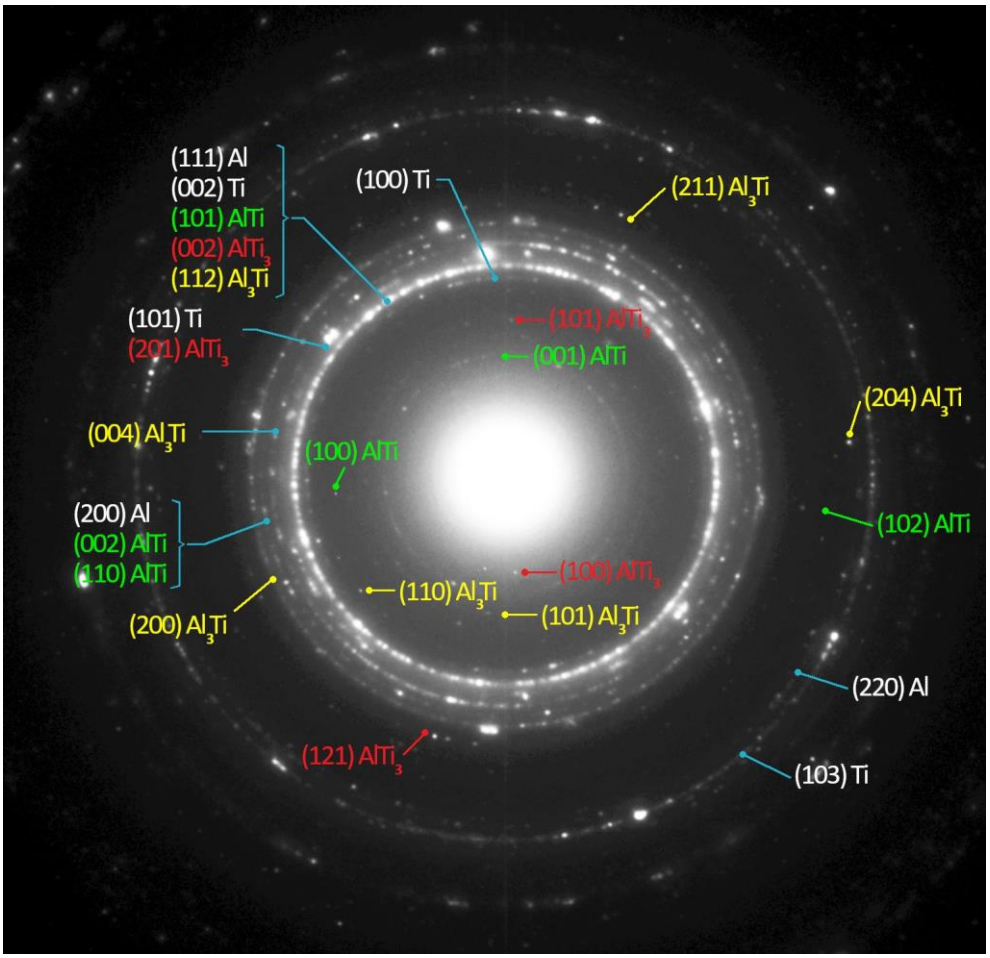

Fig. 9 SAED pattern showing presence of several intermetallic phases from the Al-Ti system

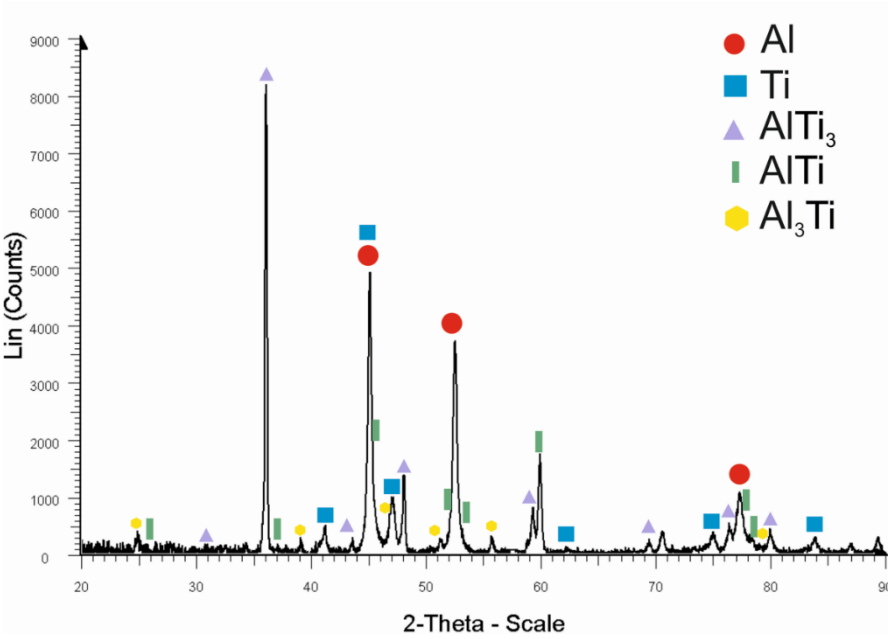

Fig. 10 XRD pattern of hybrid Al-Ti processed for 50 turns

Fig. 11 a) Microhardness distribution along the sample radius, b) Microhardness distribution across the disk in the Al-Ti sample processed for 50 turns

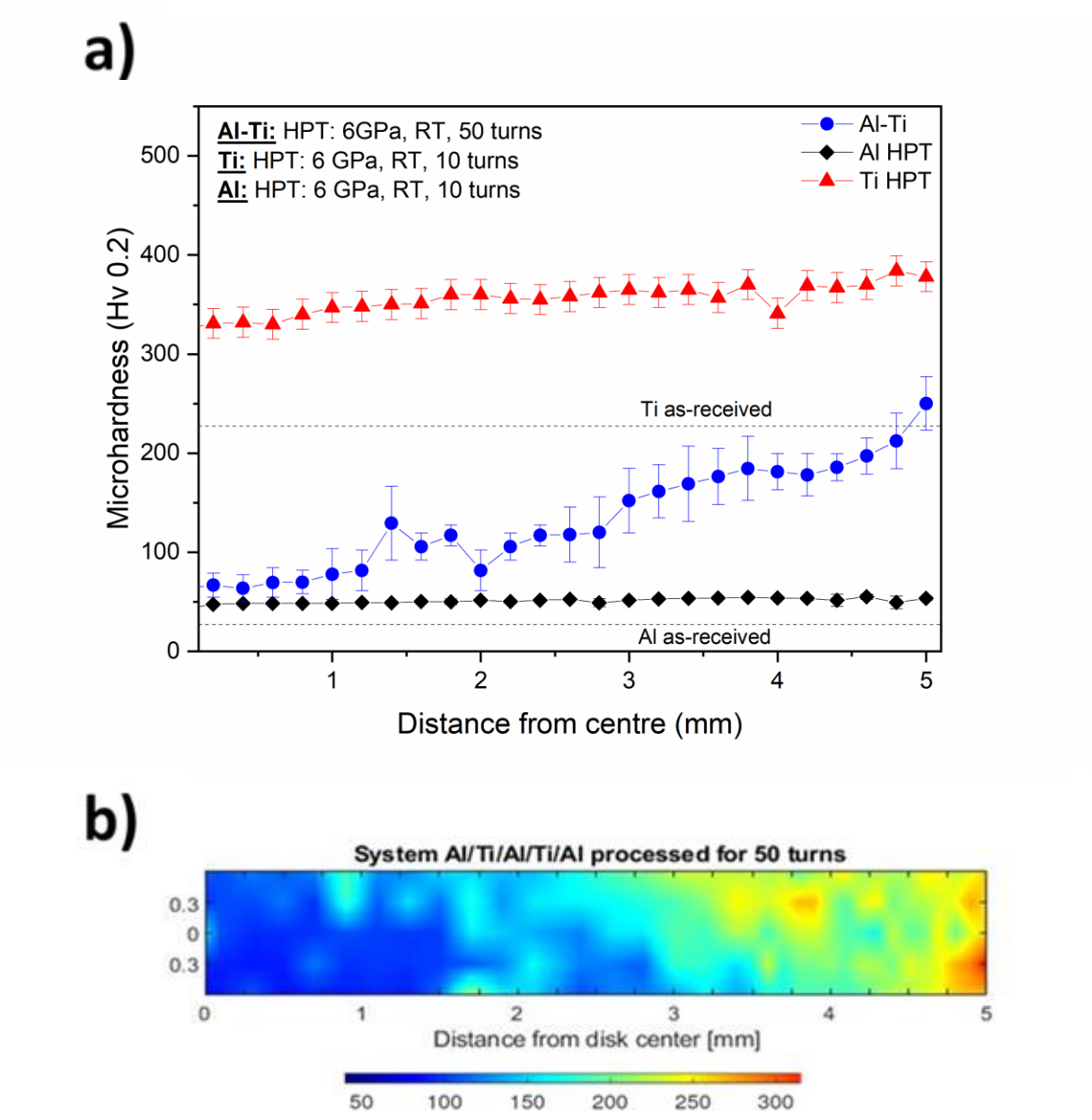

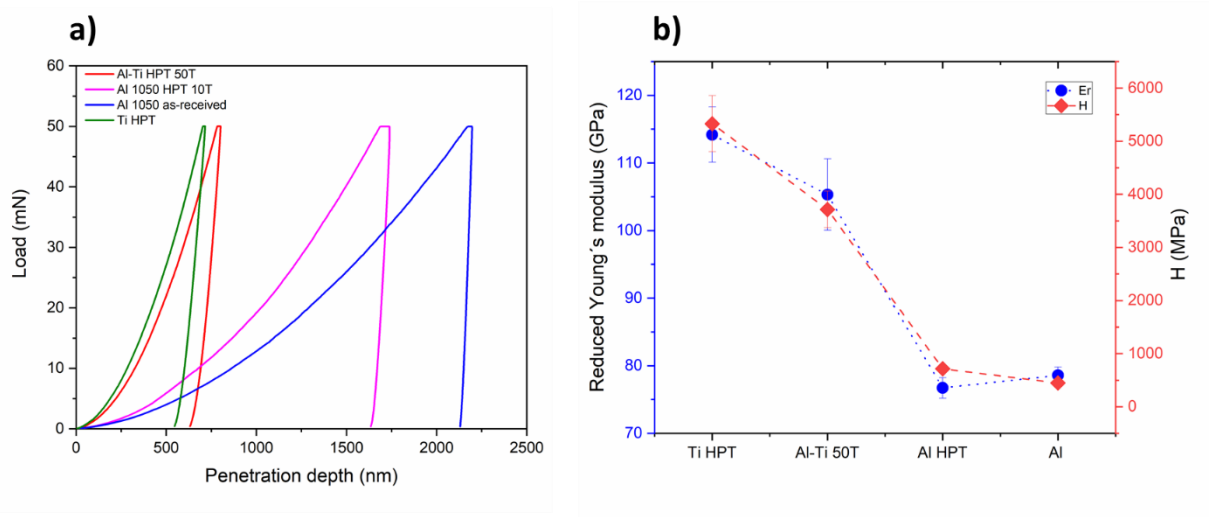

Fig. 12 a) Representative nanoindentation curves of Al-Ti hybrid material processed for 50 turns (red), Al-1050 processed for 10 turns (pink) and Al 1050 in as-received state (blue) and b) Reduced Young´s modulus and hardness of as-received and HPT-processed materials

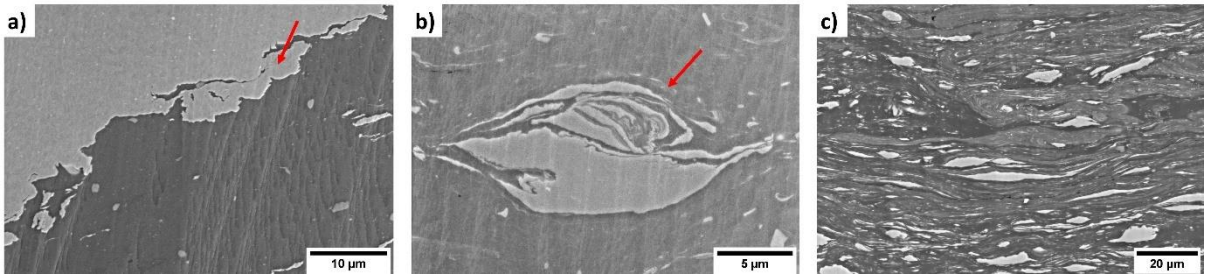

Fig. 13 Exemplary SEM images of the Al/Ti interfaces after HPT deformation

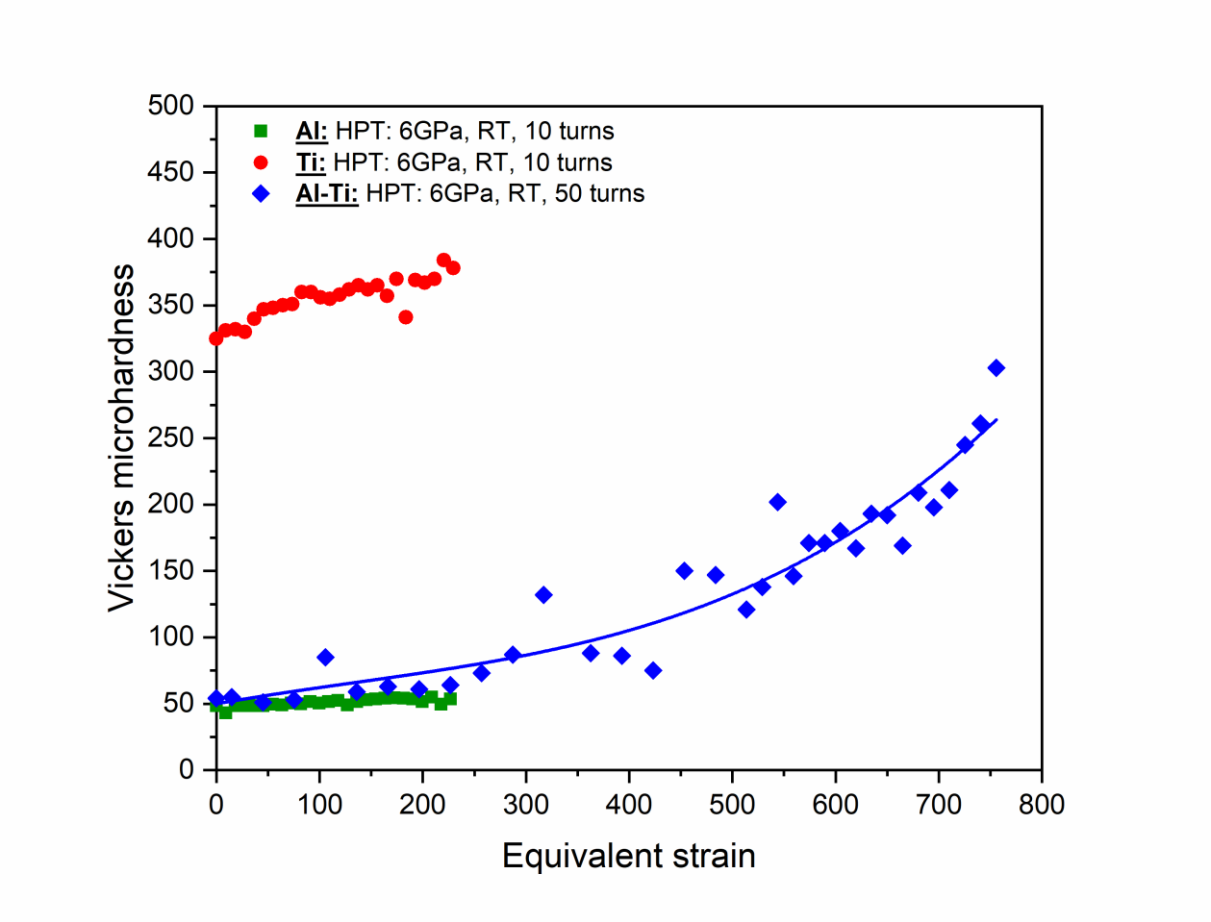

Fig. 14 Hardness as a function of accumulated strain in the Al-Ti hybrid material processed for 50 turns. HPT-processed Al-1050 and CP-Ti are added as a reference.